A model for an electromotive force generator in the magnetosphere : a source of discrete auroral arcs

M. Roth(*), D.S. Evans(**) and J. Lemaire(*)

(*) Institute for Space Aeronomy, 3 avenue Circulaire, B-1180 Bruxelles, Belgium

(**) Space Environmental Laboratory, NOAA, 325 Broadway, Boulder CO 80303, USA

Abstract

We present results obtained from solving Maxwell's and Vlasov's equations to obtain the electrical structure of the sheath which separates magnetospheric particle populations of different densities and temperatures. It is shown that for reasonable magnetospheric plasma populations an electric potential difference of several kilovolts exists across such a boundary. This potential can serve as the necessary EMF for the auroral current circuit. The colocation between a magnetospheric plasma boundary and a discrete aurora is a natural consequence of this picture.

1. Introduction

It is generally believed that discrete auroral arcs arise because of magnetic field-aligned potential differences which energize and precipitate magnetospheric electrons while retarding positive ions, so as to create a limited region of very much enhanced and electron rich energy flow to the atmosphere. It is further believed that this field-aligned potential difference occurs as a result of a source of electromotive force (EMF) located in the magnetosphere, remote from the atmosphere, and a three-dimensional current system which threads this source of EMF and the ionosphere by means of currents along the magnetic field connecting the two regions. The coincidence that often occurs between the location of a discrete auroral arc and what appears to be a boundary between two differing magnetospheric plasma populations suggests that a cause and effect relationship may be present (Ref.1).

We believe that the magnetospheric D.C. generator which drives the current in the auroral circuit results from large potential differences produced at the interface between hot plasmasheet clouds and the cooler magnetotail background plasma.

In section 2, a kinetic model describing these potential layers will be described. It is based on a kinetic theory of tangential discontinuities (TD). Results are obtained from solving Maxwell's and Vlasov's equations to give the electrical structure of the sheath which separates particle populations of different densities and temperatures. Parameters of the model and boundary conditions will be specified in section 3 for a typical magnetospheric potential layer. In section 4, it will be shown that, for reasonable magnetospheric plasma populations, an electric potential difference of many kilovolts exists across such a boundary. This potential can serve as the necessary EMF for the auroral current circuit, as will be shown in the conclusions of section 5.

The analog of this magnetospheric D.C. generator is the contact potential difference produced at the interface between two metallic conductors at different temperatures. There are also other devices and mechanisms to produce, both in the laboratory as well as in space, large potential differences and to drive currents ; e.g. the dynamo effect resulting from the motion of a conductor or of an extended cloud of plasma in a direction perpendicular to the ambiant magnetic field. In this case, the electric field is equal to the convection electric field and extends over the whole volume of the moving plasma. Unless the latter moves with a velocity larger than the uncommonly

value of 100 km/s, this convection electric field does not exceed 4 mV/m in a magnetic field of 40 nT. Charge separation thermoelectric field can however have larger values (100 - 200 mV/m) but it will be shown that they are confined in much thinner layers at the edges of plasma irregularities.

2. A kinetic model of the magnetospheric D.C. generator

Equilibrium configurations of TD in collisionless plasmas have been discussed by a number of authors in the context of thermonuclear containment (Refs. 2, 3, 4, 5, 6). Models of TD were also developed to describe the microscopic structure of current sheets in space plasmas. Kinetic theories were elaborated for the purpose of explaining the structure of the earth's plasmapause (Ref.7), of current sheets in the solar wind (Refs. 8, 9, 10) and of the terrestrial magnetopause (Refs 11, 12, 13, 14, 15, 16).

The model developed by Roth (Refs. 14, 17) considers the structure of steady-state TD in a collisionless magnetized plasma with multiple particle species. It includes changes in magnetic field intensity and direction, plasma bulk velocity, composition, temperatures and anisotropies. It is not restricted to exactly charge-neutral layers. In some cases, the role of collisions as prime mover for the dissipation is played by wave-particle interactions which determine the stability and thickness of the current layers (Refs. 13, 14). However, a simplified version of this model, a slightly modified version of Sestero's model (Ref. 5), is sufficient to describe the potential layer involved in the auroral circuit.

It is a very good approximation to consider that the radius of curvature of the current layer is much larger than its characteristic thickness, which is of the order of a few ion gyroradii. Although the plasmasheet is rarely in a steady-state, the assumption of stationarity is made and is justified by the fact that the structure of the potential layer does not change significantly over the characteristic period of time required for an Alfven's wave to cross the transition. Therefore, steady-state, unidimensional plasma current layers are considered which are parallel to the (y-z) plane of a cartesian coordinate system. All plasma and field variables are assumed to depend on the x-coordinate, normal to the layer. The magnetic field ($\tilde{B}$) is oriented along the z-axis while the electric field ($\tilde{E}$) is parallel to the x-axis. The assumption that $\tilde{B}$ does not change direction across the transition is reasonable, since the direction of the magnetospheric field at the plasmasheet cloud boundary does not change significantly. On both sides of the layer, it is also assumed that each plasma species is at rest with identical asymptotic temperatures. The asymptotic temperature of a given plasma species is however only significative on one side of the transition, since the corresponding number density will always vanish on the other side (see further, table I). Of course, inside the transition, the number density, mean velocity and temperature of the particles are generally changing. If restricted to a two-components hydrogen plasma, with a common asymptotic temperature for electrons and protons, identical on both sides, the model considered here would be identical to the one developed by Sestero (Ref. 5), for which neither electrons nor protons were allowed to have a vanishing number density either at $x = -\infty$ or at $x = +\infty$.

Because of the orientation of $\tilde{E}$ and $\tilde{B}$, the z-velocity component for a charged particle is a constant and we are therefore free to consider the motion of this particle to be in the (x-y) plane. In this plane, a charged particle has two constants of motion :

1) the energy : $H = \frac{1}{2} m (v_x^2 + v_y^2) + Ze\phi(x)$
where Ze is the charge of a particle with mass m ($e = 1.6 \times 10^{-19} C$) and $\phi(x)$ is the electric potential.

2) the y-component of the generalized momentum : $p = mv_y + Zea(x)$ where a(x) is the vector potential (oriented along the y-axis).

Because z is an ignorable coordinate, the velocity distribution function can be considered as a function of x, v_x and v_y. On the other hand, any function of H and p, F(H, p), is a solution of the steady-state Vlasov equation. To evaluate moments of F, we have to transform the (v_x, v_y) plane to the (H, p) plane. Each half of the (v_x, v_y) plane corresponding to $v_x < 0$, is mapped into the same domain, given by :

$$-\infty < p < +\infty$$

$$H_o \leq H < +\infty$$

with

$$H_o(p, x) = Ze\phi(x) + \frac{1}{2m}\left(p - Zea(x)\right)^2 \qquad (1)$$

The energy equation can also be written as

$$H = \frac{1}{2} mv_x^2 + \frac{1}{2m}(p - Zea)^2 + Ze\phi = \frac{1}{2} mv_x^2 + H_o(p, x) \qquad (2)$$

From equation (2), it can be seen that the motion is that of a particle in the potential well H_o. This means that the entire motion of a particle with constants H and p lies within the bounded interval on the x-axis determined by $H_o(p, x) \leq H$. This means that <u>all particles are trapped</u> in this model. There are no "free" particle able to escape at $\pm\infty$. F(H, p) can be chosen as arbitrary functions of their arguments and depend no longer explicitly on x. However, the number of trajectories with a given H and p determines the number of particles on the x-interval determined by $-H_o(p, x) \leq H$.

Consider the following distribution function (Ref. 5) for a given plasma species :

$$F(H, p) = \delta(p)\eta(H) \qquad (3)$$

with

$$\delta(p) = C_1 \text{ if } p \text{ in }]-(\text{sign } Z)\infty, 0] \qquad (\text{sign } Z = +1, \text{ if } Z > 0$$

$$= C_2 \text{ if } p \text{ in } [0, +(\text{sign } Z)\infty[\qquad = -1, \text{ if } Z < 0)$$

where C_1, C_2 are arbitrary (≥ 0) constants and $\eta(H)$ a Maxwellian distribution given by :

$$\eta(H) = \alpha\left(\frac{m}{2\pi kT}\right) \exp\left(-\frac{H}{kT}\right) \qquad (4)$$

where T is the asymptotic temperature of the particle species (assumed to be identical on both sides of the layer) and α is a parameter which has the dimension of a number density.

From equations (3) and (4), the number density (n) and the current density (oriented along the y-axis) can be computed as a function of ϕ and a. It is found :

$$n = \frac{\alpha}{2} \exp\left(-\frac{Ze\phi}{kT}\right)\left[C_1 \operatorname{erfc}\left(\frac{a}{RB}\right) + C_2 \operatorname{erfc}\left(-\frac{a}{RB}\right)\right. \qquad (5)$$

$$j = \frac{1}{2} |Z| e\alpha(C_2 - C_1)\left(\frac{2kT}{\pi m}\right)^{1/2} \exp\left(-\frac{Ze\phi}{kT}\right) \exp\left(-\frac{a^2}{R^2B^2}\right) \qquad (6)$$

where erfc is the complementary error function

$$\operatorname{erfc}(u) = \frac{2}{\sqrt{\pi}} \int_u^{+\infty} e^{-x^2} dx$$

and RB is a constant given by

$$RB = \left(\frac{2mkT}{Z^2e^2}\right)^{1/2} \qquad (7)$$

with R and B being some characteristic Larmor radius and magnetic field, respectively, i.e.,

$$RB = R_1B_1 = R_2B_2 \qquad (8)$$

Here R_1 and R_2 are the characteristic Larmor radius at $x = -\infty$ and $x = +\infty$, respectively ; while B_1 and B_2 are the characteristic magnetic fields at $x = -\infty$ and $x = +\infty$, respectively.

The Maxwell's equations to solve are

$$\frac{d^2\phi}{dx^2} = -\frac{e}{\varepsilon_o} \sum_{\nu=1}^{s} Z^{(\nu)} n^{(\nu)} \tag{9}$$

$$\frac{d^2a}{dx^2} = -\mu_o \sum_{\nu=1}^{s} j^{(\nu)} \tag{10}$$

where ε_o and μ_o are the vacuum permittivity and permeability, respectively ($\varepsilon_o = 8.854 \times 10^{-12}$ F/m, $\mu_o = 4\pi \times 10^{-7}$ H/m) and s, the number of particle species.

The electric field, (E,0,0) and the magnetic field (0,0,B) are derived from potentials, i.e.,

$$E = -\frac{d\phi}{dx} \tag{11}$$

$$B = \frac{da}{dx} \tag{12}$$

The magnetic and electric structures of a transition are then determined by solving the system of differential equations (9) to (12) with $n^{(\nu)}$ and $j^{(\nu)}$ given by equations (5) and (6) respectively. This can be achieved by numerical methods using a Hamin's predictor-corrector scheme. However, to obtain the electric potential ϕ, we have replaced Poisson's equation (9) by the quasi-neutrality approximation.

$$\sum_{\nu=1}^{s} Z^{(\nu)} n^{(\nu)}(a,\phi) = 0 \tag{13}$$

This approximation holds if the charge density, proportional to the Laplacian of ϕ, is found much smaller than the charge density associated with the positive (or negative) particles. Each time this condition is fulfilled, a self-consistent potential is obtained. To solve equation (13) we have used Newton's method of successive iterations.

As moments of arbitrary order (such as temperature, pressure tensor, energy flow vector...) can also be determined analytically as a function of ϕ and a (Refs. 14 and 17), a complete description of the microscopic structure of the current sheet can be achieved. It could also be shown that the well-known pressure balance condition across the layer resulting from the law of momentum conservation is retrieved in all cases.

3. The potential layer

The temperature $\theta(x)$ and density $n(x)$ of each plasma species vary across the potential layer separating the hot plasmasheet cloud at $x = -\infty$ from the cooler background magnetotail plasma at $x = +\infty$. This layer has plasma boundary conditions characterized by 8 plasma parameters as listed in table I.

Table I

ν	Z	species	$\theta(\pm\infty)$	$n(-\infty)$	$n(+\infty)$	C_1	C_2
1	-1	e_{sh}	T^-_{sh}	N^-_{sh}	0	1	0
2	-1	e_t	T^-_t	0	N^-_t	0	1
3	+1	p_{sh}	T^+_{sh}	N^+_{sh}	0	1	0
4	+1	p_t	T^+_t	0	N^+_t	0	1
			(eV)	(cm^{-3})	(cm^{-3})		

These plasma parameters correspond to two interpenetrated hydrogen plasmas with different characteristics. In table I, the upper indices - and + refer to electrons and protons, respectively, while the lower indices sh and t refer to the plasmasheet cloud and background magnetotail particles, respectively. The values of the parameters C_1 and C_2 are also given in this table. From equation (3), it can be seen that they are consistent with the fact that the plasmasheet cloud (/magnetotail) particles are absent on the magnetotail (/plasmasheet cloud) side.

To obtain the number densities for this potential layer, let us first define :

$$\frac{a}{R_1^{(1)} B_1} = G$$

$$R_1^{(\nu)}/R_1^{(1)} = R_2^{(\nu)}/R_2^{(1)} = r^{(\nu)}$$

From equations (5) and (6), the number densities (n) for each species can be written down.

$$n^-_{sh} = \frac{1}{2}\alpha^-_{sh} \exp\left(\frac{\phi}{T^-_{sh}}\right) \operatorname{erfc}(G) \qquad (14)$$

$$n^-_t = \frac{1}{2}\alpha^-_t \exp\left(\frac{\phi}{T^-_t}\right) \operatorname{erfc}\left(-\frac{G}{r^-_t}\right) \qquad (15)$$

$$n^+_{sh} = \frac{1}{2}\alpha^+_{sh} \exp\left(-\frac{\phi}{T^+_{sh}}\right) \operatorname{erfc}\left(\frac{G}{r^+_{sh}}\right) \qquad (16)$$

$$n^+_t = \frac{1}{2}\alpha^+_t \exp\left(-\frac{\phi}{T^+_t}\right) \operatorname{erfc}\left(-\frac{G}{r^+_t}\right) \qquad (17)$$

In equations (14) through (17), ϕ is in volt, T in eV and α in cm^{-3}.

Let us now choose the electric potential at $x = -\infty$ equal to zero, i.e.

$$\phi_1 = \phi(-\infty) = 0 \qquad (18)$$

Then, the parameters α in equations (14) through (17) can be seen to be related to the asymptotic densities and to the value of ϕ at $x = +\infty$ (ϕ_2). Taking into account of the plasma neutrality at $x = \pm\infty$

$$N^-_{sh} = N^+_{sh} = N_{sh} \qquad (19)$$

$$N^-_t = N^+_t = N_t \qquad (20)$$

one obtains (assuming that B> 0, so that $G(-\infty) = -\infty$; $G(+\infty) = +\infty$)

$$\alpha^-_{sh} = \alpha^+_{sh} = N_{sh} \qquad (21)$$

$$\alpha^-_t \exp\left(\frac{\phi_2}{T^-_t}\right) = \alpha^+_t \exp\left(-\frac{\phi_2}{T^+_t}\right) = N_t \qquad (22)$$

From equation (22), it can be seen that α_t^-, α_t^+ or ϕ_2 can be chosen as an arbitrary parameter. In the following section, we will describe a potential layer corresponding to a value of ϕ_2 equal to 0 V. The plasma and magnetic field parameters for that layer are listed in table II, where B_{sh} denotes the value of the magnetic field at $x = -\infty$, i.e. deeply inside the plasmasheet cloud.

TABLE II

N_{sh}^-	T_{sh}^-	N_{sh}^+	T_{sh}^+	N_t^-	T_t^-	N_t^+	T_t^+	B_{sh}
0.5	2500	0.5	12000	0.15	800	0.15	3000	40
cm^{-3}	eV	cm^{-3}	eV	cm^{-3}	eV	cm^{-3}	eV	nT

4. Numerical results

The numerical programme is based on the theory developed in this paper. It determines the vector potential a and the electric potential ϕ by solving the Maxwell equation (10) as well as the equation describing the quasi-neutrality approximation (13). Furthermore, this programme computes the moments of the velocity distribution functions, which have been determined analytically in terms of a and ϕ up to the third order (Refs. 14 and 17). It also computes the magnetic field B (Eq.12), the electric field E (Eq.11) and associated charge density, thus leading to a complete description of the internal structure of the layer. Equations (10) and (12) form a system of two differential equations of the first order for a and B, which has been integrated numerically by using a Hamin's predictor-corrector scheme (Ref.18). In practice, one starts integrating with a large negative value of a so that the asymptotic moments of the velocity distribution functions at $x = -\infty$ are reached.

Figure 1 illustrates the case of a potential layer for which $\phi_2 = 0$. It can be seen that two different scale lengths characterize the structure of the transition. At both ends, the ion gyroradius ($R^+ = 280$ km) is the representative scale length, while the electron gyroradius ($R^- = 3$ km) dominates the middle of the transition. This very thin structure - about 4 electron gyroradii thick - is mainly an electron-dominated layer, i.e., a layer dominated by the electron current. This layer is illustrated in panels of the 2nd and 4th columns.

Panels of the 1st and 3rd columns illustrate the characteristics of two much thicker transitions, dominated by the ion current. These ion-dominated layers are separated by the thin electron-dominated layer located near $x \simeq 0$. In the panels describing the two ion-dominated layers located at both ends of the sheath, the lack of continuity that apparently occurs in drawing the curves does not represent a true or mathematical discontinuity. The numerical computation was really performed from $x = -x_o$ to $x = +x_o$ ($x_o >> 1\ R^+$) and the integration step was adjusting itself to sharp variations in a and B as a result of the Hamin's procedure. Actually, the structure of the very thin electron-dominated layer could not be displayed on the much larger scale of the ion-dominated layers and, on that scale, has been removed for more clearness.

For both kinds of layer (displayed side by side), from top to bottom and from left to right, figure 1 illustrates respectively : the electric potential (ϕ), the electric field ($E_x = E$), the relative charge separation ($dQ/Q = -[\varepsilon_o d^2\phi/dx^2]/n^+ e$), the electric field in the plasma frame ($E_x = E_x + C_y B_z$, where C_y is the plasma bulk velocity), the electron (e) and proton (p) average velocity (V_y), the quantity A corresponding to the threshold for the lower-hybrid drift instability (Ref.19) [$A = |V_y^+ - V_y^+|/U^+$ where U^+ is the average thermal ion speed : $U^+ = (k\theta^+/m^+)^{1/2}$] ; the electron ($e_{sh}$) and proton ($p_{sh}$) densities (n) of the plasmasheet cloud particles, the electron (e_t) and proton (p_t) densities (n) of the magnetotail background ; the total electron (e)/proton (p) density (n), the temperature (θ) of each plasma species (i.e. for the electrons (e_{sh}) and protons (p_{sh}) of the plasmasheet cloud as well as the electrons (e_t) and protons (p_t) of the magnetotail background) ; the temperatures (θ) of the electrons (e) and protons (p), obtained by averaging on both electron and proton species, respectively ; and finally the magnitude of the magnetic field ($B_z = B$).

From figure 1, it can be seen that the potential difference on both sides of the electron-dominated layer is about 1350 V (see panels of ϕ displayed on both ion and electrons scales). The charge separation electric field normal to the surface of the plasma sheath has a peak value of 220 mV/m inside the electron-dominated layer (see panel of E_x displayed on the R-scale) but does not exceed 2.5 mV/m inside the ion-dominated layers (see corresponding panels displayed on the R^+ scale). Note the large ion velocity jets of more than 500 km/s inside the ion-dominated layers (see panels of V_y displayed on the R^+ scale). These jets are parallel to the plasma sheath and perpendicular to the magnetic field and occur on a scale length of about 300 km. As might be expected,

these ion jets represent the main contribution to the electric current in the ion-dominated layers. In these layers, the neutralizing electrons have guiding centers penetrating further than the ion guiding centers, towards the "sides of lower density" (towards $x = 0\ R^+$ and towards $x = 5\ R^+$). This gives rise to negatively charged layers near $x = -1\ R^+$ and $x = +1\ R^+$ (see panels of dQ/Q displayed on the R^+ scale). At these locations, a positive electric field (~ 2mV/m) sets up (see panel of E_x displayed on the R^+ scale) which tends to reduce further the charge separation. As a consequence, for several hundred kilometers, this weak charge separation electric field accelerates the ions in a direction normal to the sheath, towards the "sides of lower density". These ions are finally deflected transversely by the magnetic field just as they attain a maximum kinetic energy (near $x = 0$ and $x = 0.5\ R^+$). Therefore, the ions acquire a large transverse velocity (V_y) parallel to the sheath (~ 500 km/s) that greatly exceeds that of the electrons (see panel of V_y displayed on the R^+ scale). Note also that, in the two ion-dominated layers located at both ends of the potential layer, the density gradient is parallel to the potential gradient (see panels of n and ϕ displayed on the R^+ scale).

On the other hand, a narrow jet of electrons is found inside the electron-dominated layer (see panel of V_y displayed on the R^- scale). This jet has a peak value of more then 10,000 km/s and represents of course the main contribution to the electric current in the electron-dominated layer near $x \simeq 0$. In this layer (see panels displayed on the R^- scale), and quite similarly to the classical Ferraro magnetopause (Ref.20), the positive ions tend to penetrate more deeply towards the "side" of lower density (towards $x = +4\ R^-$) than the electrons. This produces a strong polarization electric field (see panel of E_x displayed on the R^- scale) perpendicular to the magnetic field and a layer of positive charges between $x \simeq -0.5\ R^-$ and $x \simeq 2.5\ R^-$ (see panel of dQ/Q displayed on the R^- scale). The strong electric field near $x \simeq 0$ opposes the charge separation to maintain the quasi-neutrality. The electrons are accelerated by this strong electric field in a direction normal to the sheath and are finally deflected transversely by the magnetic field just as they attain a maximum kinetic energy, a fraction of the thermal energy of the ions from the plasmasheet cloud. Therefore, these electrons acquire a very large velocity (V_y) parallel to the sheath (~ 10,000 km/s) that greatly exceeds that of the ions (see panel of V_y displayed on the R^- scale).

It is also interesting to note that E'_x takes large values, even in the ion-dominated layers (~ 30 mV/m). This means that the ideal MHD approximation is not applicable here, otherwise $E'_x = E_x + C_y B_z$ should vanish. In the electron-dominated layer, (see panel of E_x and E'_x displayed on the R^- scale), $E'_x \sim E_x$ and the electric field (E_x) is mainly a charge separation electric field.

The ion-dominated layers are seen to be stable, at least with respect to the lower-hybrid drift instability. Indeed at both ends of the potential layer (see panel of A displayed on the R^+ scale), the quantity A is everywhere less than 1, the corresponding threshold. However, the thin electron-dominated layer, near $x \simeq 0$, is highly instable since $A \gg 1$ (see panel of A displayed on the R^- scale) and likely to produce large amplitude electrostatic wave noise. These waves can then interact with the electrons by changing their pitch angle distribution. As a result of this wave-particle interaction, the initially anisotropic electron velocity distribution becomes more isotropic and the electron-dominated layer tends to broaden.

Note also the diamagnetic effect (see panel of B_z) due to the surface current around the plasmasheet cloud. The decrease of the magnetic pressure inside the plasmasheet cloud is, of course, balanced by an equivalent increase in the kinetic plasma pressure inside the cloud, as the magnetic + kinetic pressure does not change across the sheath.

Finally, it is important to see that the relative charge separation (see panels of dQ/Q) is smaller than 2% within the electron-dominated layer and smaller than 3×10^{-6} in the adjacent ion-dominated layers. This confirms a posteriori that charge-neutrality is satisfied to a very good approximation. This confirms also that the solution for $\phi(x)$ is a satisfactory approximation for the electric potential distribution throughout the whole transition. A test has also been made to check the validity of the charge neutrality equation(13).This equation was then replaced by :

$$\sum Zn(a,\phi) = n^{+}\varepsilon \qquad (23)$$

where ε was chosen to be the maximum value of $|dQ/Q|$ obtained from figure 1. It was found that the resulting electric field was not significantly different from the one obtained in figure 1, even in the very thin electron-dominated layer.

5. Conclusions

The electric potential (ϕ) and electric field (E_x) structures of a potential layer are illustrated in figure 2 for different values of $\phi_2 - \phi_1 = \phi_2$, i.e. for different values of the electric potential difference across the sheath (+ 3500 V, 0 V, - 1650 V and - 3500 V). The left-hand side panels characterize the ion-dominated layers, located at both ends of the potential layer, while the right-hand side panels pertain to the thin electron-dominated layer, near x = 0. The boundary conditions are the same as those given in table II. As for figure 1, the structure of the very thin electron-dominated layer near x = 0 is not displayed on the much larger scale of the ion-dominated layers (left-hand side panels).

It can be seen that one can generate a wide variety of electric potential (and electric field) structures. These layers are illustrative examples for a magnetospheric EMF source. It is important to note that $\phi(x)$ is not constant, even when $\phi_2 - \phi_1 = 0$. The large perpendicular electric fields generated across the thin electron-dominated layers will be smoothed irreversibly by the wave-particle diffusion mechanism mentioned in the previous section. When mapped down in the ionosphere, these large perpendicular magnetospheric electric fields, must drive very large Pedersen and Hall electric currents through the resistive ionosphere. These currents are dissipated by Joule heating and this leads to enhance the local electric conductivity. The large potential gradients (1-2 kV) applied across the magnetospheric potential layers are then dissipated as the ionospheric resistance becomes vanishingly small. Magnetospheric potential differences (EMF) perpendicular to magnetic field lines become then field-aligned potential differences accelerating auroral electrons downwards along auroral arc magnetic field lines. To aliment this source of auroral electron precipitation it is necessary, however, to maintain the electron-dominated layer unstable for the whole life time of the discrete auroral arc. Therefore, the plasma layer must constantly be reforming, for instance by convection of the plasma cloud 'surfing' earthward in the ambiant magnetospheric background.

The characteristic scale of variation of the electric potential is the average ion Larmor radius for the broadest structure of a magnetospheric potential layer ; i.e. 500-800 km. Its extent projected in the ionosphere is however 30 times smaller, i.e. 15-30 km. This corresponds almost to the typical latitudinal width of a discrete auroral arc.

6. References

1. LYONS, L.R. and EVANS, D.S., An association between discrete aurora and energetic particle boundaries, J. Geophys. Res., 1984, 89, 2395-2400.
2. HARRIS, E.G., On a plasma sheath separating regions of oppositely directed magnetic field, Nuovo Cimento, 1962, 23, 115-121.
3. NICHOLSON, R.B., Solution of the Vlasov equations for a plasma in a uniform magnetic field, Phys. Fluids, 1963, 6, 1581-1586.
4. KAN, J.R., Equilibrium configurations of Vlasov plasmas carrying a current component along an external magnetic field, J. Plasma Phys., 1972, 7, 445-449.

5. SESTERO, A., Structure of plasma sheaths, Phys. Fluids, 1964, 7, 44-51.
6. SESTERO, A., Vlasov equation study of plasma motion across magnetic fields, Phys. Fluids, 1966, 9, 2006-2013.
7. ROTH, M., The plasmapause as a plasmasheath : a minimum thickness, J. Atmos. Terr. Phys., 1976, 38, 1065-1070.
8. LEMAIRE, J. and BURLAGA, L.F., Diamagnetic boundary layers : a kinetic theory, Astrophys. Space Sci., 1976, 45, 303-325.
9. BURLAGA, L.F. and LEMAIRE, J., Interplanetary magnetic holes : theory, J. Geophys. Res., 1978, 83, 5157-5160.
10. ROTH, M., A computer simulation study of the microscopic structure of a typical current sheet in the solar wind, in "The Sun and the Heliosphere in Three Dimensions", ed. R.G. Marsden, D. Reidel Publishing Company (Astrophysics and Space Science Library), 1986, 167-171.
11. ALPERS, W., Steady state charge neutral models of the magnetopause, Astrophys. Space Sci., 1969, 5, 425-437.
12. ROTH, M., Structure of tangential discontinuities at the magnetopause : the nose of the magnetopause, J. Atmos. Terr. Phys., 1978, 40, 323-329.
13. ROTH, M., A microscopic description of interpenetrated plasma regions, Proceedings of Magnetospheric Boundary Layers Conference, Alpbach, 11-15 June 1979, edited by B. Battrick and J. Mort, ESTEC, Noordwijk, The Netherlands, ESA SP-148, 1979, 295-309.
14. ROTH, M., La structure interne de la magnétopause, Ph.D. Thesis, Brussels Univ., Aeronomica Acta A, 1980, n°221, also in : Académie Royale de Belgique, Mémoire de la Classe des Sciences, Collection in 8°-2e série, 1984, T XLIV - Fascicule 7 et dernier, 222 p.
15. LEE, L.C. and KAN, J.R., A unified kinetic model of the tangential magnetopause structure, J. Geophys. Res., 1979, 84, 6417-6426.
16. WHIPPLE, E.C., HILL, J.R. and NICHOLS, J.D., Magnetopause structure and the question of particle accessibility, J. Geophys. Res., 1984, 89, 1508-1516.
17. ROTH, M., Boundary layers in space plasmas : a kinetic model of tangential discontinuities, Proceedings of the XVI International Conference on Phenomena in Ionized Gases, Düsseldorf, Eds. W. Bötticher, H. Wenk and E. Schulz-Gulde, 1983, 139-147.
18. RALSTON, A. and H.S. WILF, Méthodes mathématiques pour calculateurs arithmétiques, Dunod, Paris, 1965, 482 p.
19. McBRIDE, J.B., OTT, E., BORIS, J.P. and ORENS, J.H., Theory and simulation of turbulent heating by the modified two-stream instability, Phys. Fluids, 15, 1972, 2367-2383.
20. WILLIS, D.M., Structure of the magnetopause, Rev. Geophys. Space Phys., 1971, 9, 953-985.

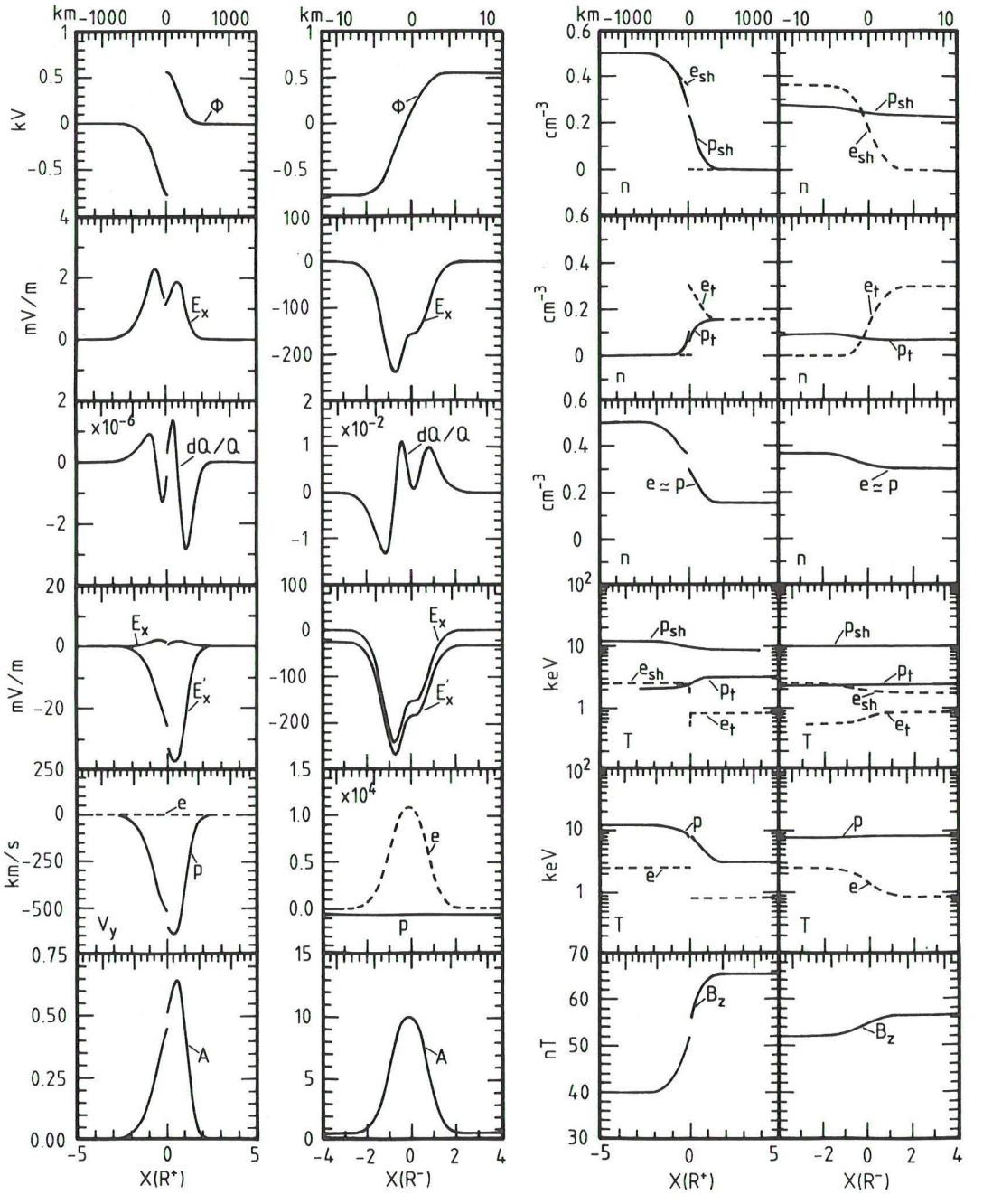

Figure 1 : Structure of a potential layer for which $\phi_2 - \phi_1 = 0$ V. Boundary conditions are given in table II. At both ends of this potential layer (see panels of the 1st and 3rd columns displayed on the R^+ scale), the ion gyroradius ($R^+ = 280$ km) is the representative scale length, while the middle of the transition (see panels of the 2nd and 4th columns displayed on the R^- scale) is dominated by a very thin structure, whose scale length is the electron gyroradius ($R^- = 3$ km). Note that the structure of this very thin electron-dominated layer, centered near x = 0 can not be displayed on the much larger scale of the adjacent ion-dominated layers and, on that scale, has been removed for more clearness. See text for details.

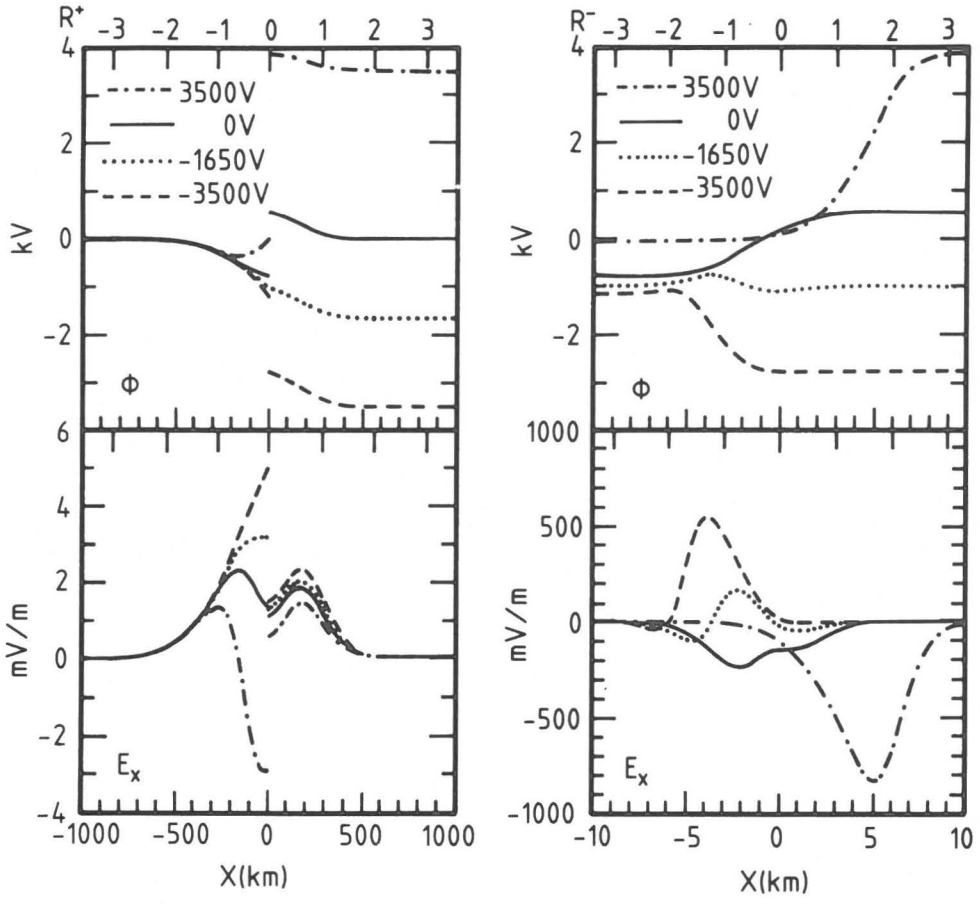

Figure 2 : Electric potential (ϕ) and electric field (E) structures for different values of $\phi_2 - \phi_1$ (+ 3500 V, 0 V, - 1650 V and - 3500 V). The left-hand side panels characterize the ion-dominated layers, located at both ends of the sheath, while the right-hand side panels pertain to the thin electron-dominated layer near x = 0. Boundary conditions are given in table II. As in figure 1, the structure of the very thin electron-dominated layer near x = 0 is not displayed on the much larger scale of the ion-dominated layers (left-hand side panels).

DISCUSSION

C.G.Fathammar,NO

How do you envisage the extremely sharp edge of the cloud to be established?

Author's Reply

Electron sheaths imbedded within the broad ion transition are unstable with respect to the lower-hybrid drift instability. Because of wave-particle interactions within these electron sheaths, these thin transitions tend to broaden and eventually to disappear when the velocity distribution of electrons has become isotropic within the plasma cloud and in the ambiant background plasma. This instability is a source for the pitch angle scattering of electrons. To eliminate the source of electron precipitations you have to maintain the electron sheath unstable for the whole life time of the discrete auroral arc, and consequently the electron layer must be constantly reforming, for instance, by convection of the cloud in the ambiant magnetotail.

E.C.Whipple,US

Would the author explain in more detail how the electrostatic potential developed across a boundary layer can develop into a magnetic field-aligned potential drop?

Author's Reply

The large perpendicular magnetospheric electric fields generated within the very thin electron layer, when mapped into the ionosphere, will drive very large Pedersen and Hall currents through the resistive ionosphere. The Joule dissipation of these curren increases the local plasma temperature. The local ionization density is then enhanced not only by the increased plasma temperature, but also by primary auroral electron bombardment. All these effects concur to enhance the local electric conductivity and to short-circuit the ionospheric load. The magnetospheric electrostatic potential is then discharged as the ionospheric resistance becomes vanishingly small. Perpendicular magnetospheric potential differences become then field-aligned potentia differences accelerating auroral electrons downwards along auroral arc magnetic field lines.